Mater Eng Res, 2021, 3(1): 165-174
DOI: 10.25082/MER.2021.01.005

RESEARCH ARTICLE

Carburization effect of austenitic alloys with various Cr and Al additions under the methane/hydrogen atmosphere on the corrosion behaviors of steels

Shu Liu[1] **Jing Cui**[1*]

[1] Industrial Training Centre, Shenzhen Polytechnic, Shenzhen 518000, China

*Correspondence to: Jing Cui, Industrial Training Centre, Shenzhen Polytechnic, Shenzhen 518000, China; Email: 2651852137@qq.com

Received: October 25, 2021;
Accepted: December 2, 2021;
Published: December 8, 2021.

Citation: Liu S and Cui J. Carburization effect of austenitic alloys with various Cr and Al additions under the methane/hydrogen atmosphere on the corrosion behaviors of steels. *Mater Eng Res*, 2021, **3**(1): 165-174. https://doi.org/10.25082/MER.2021.01.005

Abstract: The corrosion behaviors of six Fe-19Ni-13/21Cr-*x*Al (*x* = 0, 2, 6 at. %) alloys in 10% $CH4/H_2$ at 800°C were investigated. 2 at. % Al did not affect the corrosion resistance obviously, while 6 at. % Al reduced the carbon attack completely for Fe-19Ni-13Cr-6Al but was still insufficient to form protective alumina scales for alloys with 21 at. % Cr. An increase of Cr content changed the appearance of the internal carburization zone under the optical microscope. Stability diagrams of M-C-O system (M = Cr, Fe) were established to estimate the diffusion paths of carbon in the alloys.

Keywords: Fe-Ni-Cr-Al, carburization, high temperature corrosion, carbon attack

1 Introduction

Carburization and metal dusting frequently occur on alloys exposed to the typical petrochemical environment with high carbon activities. When the alloys were exposed to the gas mixture with carbon activity (a_c) less than 1, carbon atoms could diffuse into the alloys and therefore the internal carbides formed. However, when the alloys were exposed to the aggressive environment with the carbon activities larger than 1, the surface alloy layer will be converted into mixture of carbides, carbon coke and metal particles, the integrity of the materials will be destroyed, therefore the metal dusting are always catastrophic [1, 2].

A chromia external scale could protect the substrate from the attack in oxidizing atmosphere [3, 4]. However, chromium could react with carbon and form stable carbides in alloys exposed to gas mixtures with high carbon activities. This will lead to the consumption of Cr in the subsurface zone and suppress the formation of external chromia. In addition, carbon could diffuse inwards through chromia scales via oxide grain boundaries [5–7]. Therefore, just relying on external chromia scale to obtain excellent carbon resistance is difficult. However, addition of Al could promote the formation of external alumina which is more stable than chromia and could offer a much better protection in many aggressive environments [8]. Till now, the critical Al contents needed to form protective Al_2O_3 scales in gas mixtures with high carbon activities have been widely investigated [9–11]. The corrosion behaviors of the six Fe-19Ni-13/21Cr-*x*Al (*x* = 0, 2, 6 at. %) alloys had been already studied at 900°C exposed to gas mixtures with carbon activities smaller than 1 or larger than 1 [12, 13]. Small addition of Al, which could not support the formation of continuous alumina scales, had no obvious effect on carbon attack. The corrosion resistance was highly developed by adding enough aluminum. However, addition of aluminum into the alloy could promote the formation of ferrite which is harmful for the mechanical properties [8]. Therefore, investigation on how to promote the formation of external Al_2O_3 with less Al addition is significant. In many environments, more addition of Cr will result in smaller critical Al content to form a protective alumina scale. Till now, few papers have been focused on the synergic effect between Cr and Al on the prevention of the carbon attack.

The aim of this paper is to investigate the behaviors of the model austenitic Fe-Ni alloys with various Cr and Al additions corroded in a gas mixture with a high carbon activity in the presence of trace of oxygen insufficient to form Cr_2O_3 at a high temperature. The corrosion behaviors of all alloys are compared to explore the effect of Cr, the effect of Al and the interaction between Cr and Al on the general behaviors of all alloys.

2 Materials and methods

Six alloys with nominal chemical composition (all in at. %, if not specified otherwise) Fe-19Ni-13/21Cr-xAl (x = 0, 2, 6) were prepared by vacuum induction melting using mixtures

of high purity metals (wt. %) (99.9 Fe, 99.0 Cr, 99.9 Ni, 99.7 Al) and then cast in cylinders of 5 cm diameter, 10 cm high. The alloy ingots were subsequently annealed in 1 atm argon at 1000°C for 36 h to release the residual stresses and achieve a better equilibration. The five alloys Fe-19Ni-13/21Cr, Fe-19Ni-13/21Cr-2Al and Fe-19Ni-13Cr-6Al are all single-phase fcc (γ-phase). Conversely, Fe-19Ni-21Cr-6Al, is composed of a mixture of a γ-phase matrix with precipitates evenly distributed, the Cr in the alloy accumulate in the precipitates which have similar structure to the matrix [12]. Samples were cut into 10 × 8 × 1.5 mm from the ingots using a line saw and a hole with 1 mm in diameter was drilled near one edge. All samples were mechanically abraded on successively finer abrasive papers down to 2000 grit and finally cleaned with water, acetone and ethanol and dried immediately before each test. The experiments were carried out at 800°C under 1 atm in a gas mixture of (vol.%) 10% CH_4/H_2 for 12 h in a microbalance Setaram B-92 using a Pt catalyst. The gases were premixed and dried by P_2O_5 before entering in the reaction chamber.

The carbon activity of the CH_4/H_2 mixtures used here is determined by the virtual equilibrium of the following reaction:

$$CH_4 = C + 2H_2 \tag{1}$$

according to the equation:

$$a_c = K_1 \frac{P_{CH_4}}{P_{H_2}^2} \tag{2}$$

where K_1 is the equilibrium constant for the Reaction (1), which could be calculated according to the thermodynamic data from HSC chemistry version 6.0 [14], P_{CH_4} and P_{H_2} are the actual partial pressures of the gases in the gas mixture used. The carbon activity of the gas mixture used here is equal to 2.6. The oxygen pressure listed in Table 1 was calculated according to the content of the impurities in the gas mixture, which were also given in the same table. The oxygen pressure at 800°C is below 10^{-29} atm according to factsage: this value is higher than the dissociation pressure of Al_2O_3, but lower than that of Cr_2O_3. Therefore, Al_2O_3 could form in this atmosphere on alloys containing Al, while the formation of chromia is ruled out.

Table 1 Gas mixture, calculated carbon activity and oxygen pressure for the exposure condition

CH_4(vol. %)	H_2(vol. %)	a_c	P_{O_2}*(atm)	Impurities
10	90	2.6	$\leq 10^{-29}$	$O_2 \leq 1.00$ ppm CO ≤ 0.18 ppm $CO_2 \leq 0.18$ ppm $H_2O \leq 2.90$ ppm

Notes: the oxygen pressure was calculated according to the content of the impurities in the gas mixtures

The corroded samples were examined by means of optical microscopy (OM), scanning electron microscopy (SEM), generally using the back-scattered electron image (BEI) mode, energy dispersive X-ray microanalysis (EDX), and XRD to study the structure of the scales, to identify the nature of the phases and their distribution and for elemental analysis. The reacted samples were etched with Murakami's etchant to reveal the precipitated carbides.

3 Results

3.1 Corrosion kinetics

The kinetic curves for all alloys corroded in 10% CH_4/H_2 at 800°C for 12 h are shown in Figure 1a, Figure 1b as linear plots and Figure 1c, Figure 1d as parabolic plots, respectively. After an initial stage of about 1 h, a parabolic stage appeared with a parabolic rate constant k_p equal to 9.5 × 10^{-11} $g^2cm^{-4}s^{-2}$ on Fe-19Ni-13Cr. The kinetic curve for Fe-19Ni-13Cr-2Al also obeyed the parabolic law, the curve showed a parabolic stage with k_p = 1.3 × 10^{-10} $g^2cm^{-4}s^{-2}$. The alloy Fe-19Ni-13Cr-6Al exposed to 10% CH_4/H_2 at 800°C for 12 h produced a kinetic curve which show similar performance to that of the above two alloys. An initial stage lasting from 0 to 0.8 h appeared followed by a parabolic stage with k_p = 3.2 × 10^{-14} $g^2cm^{-4}s^{-2}$. A similar behavior was shown by Fe-19Ni-21Cr, a parabolic stage lasting from 1 h to the end appeared (k_p = 9.2 × 10^{-11} $g^2cm^{-4}s^{-2}$) after the initial period. After the initial incubation periods, the kinetic curves for Fe-19Ni-21Cr-2Al and Fe-19Ni-21Cr-6Al both followed the parabolic rate law: Fe-19Ni-21Cr-2Al, lasting from 1 h to the end with k_p = 1.2 × 10^{-10} $g^2cm^{-4}s^{-2}$ and Fe-19Ni-21Cr-6Al, lasting from 1.44 h to the end with k_p = 7.0 × 10^{-13} $g^2cm^{-4}s^{-2}$.

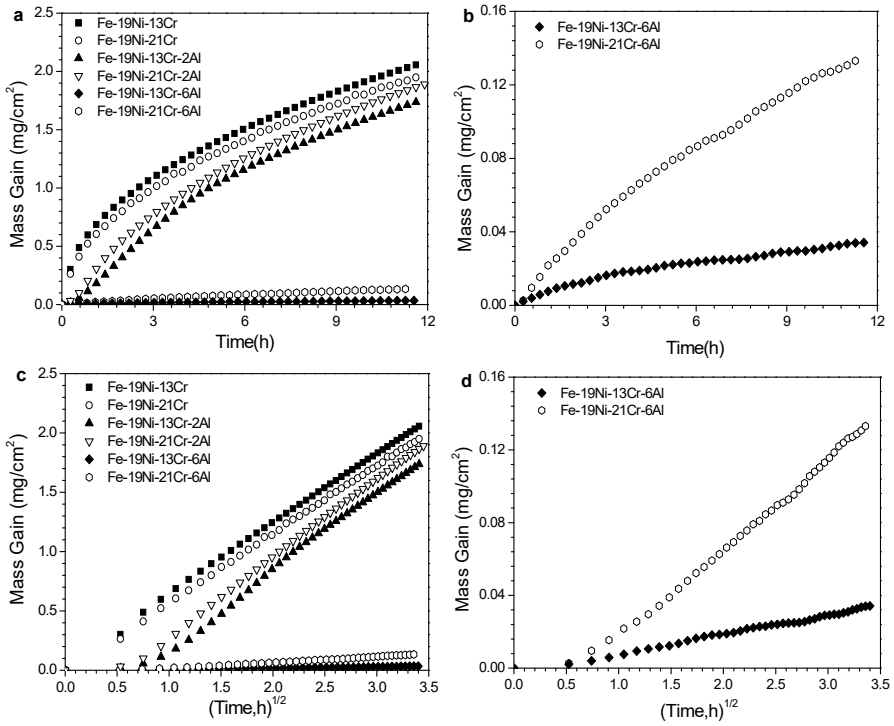

Figure 1 Kinetic curves for the corrosion of Fe-19Ni-13/21Cr-xAl in 10% CH_4/H_2 at 800°C (a_c = 2.6) for 12 h. (a): linear plots; (b): enlarged view of linear plots of Fe-19Ni-13/21Cr-6Al; (c): parabolic plots; (d): enlarged view of parabolic plots of Fe-19Ni-13/21Cr-6Al.

According to the kinetic curves, the mass gains for alloys with 6 at. % Al were significant smaller than the other alloys with the same Cr content. Therefore, addition of 6 at. % Al could improve the corrosion resistance of the alloys effectively. While this effect was not so obvious for alloys with less Al addition, the decrease of the mass gain obtained by comparing the corresponding kinetic curves for the alloys with 2 at. % Al and without Al was much smaller than that obtained from the alloys with 6 at. % Al and 2 at. % Al but with the same Cr content. In addition, the addition of Cr from 13 at. % Al to 21 at. % Al did not affect the mass gain obviously for alloys with the same Al content exposed to the gas mixture used here with the oxygen pressure insufficient to form chromia.

3.2 Morphology and structure of the scales

The metallographic examination of the cross-sections after etching by Murakami's etchant revealed a similar morphology of the internal carburization zones for Fe-19Ni-13Cr and Fe-19Ni-13Cr-2Al after corroded in 10% CH_4/H_2 at 800°C for 12 h (Figure 2 and Figure 3). According to the OM figures, the internal carburization zones for both alloys could be divided into three different layers. The carbides in the outer layer are globular which could be M_7C_3 (with M = Fe, Cr) according to the corresponding XRD results. The middle layer and the inner layer contained small and cubic carbides. However, carbides in the middle layer are too small and dense to be visible in the corresponding OM micrographs. According to the D. J. Young [15], these carbides should be $M_{23}C_6$ (with M = Fe, Cr). For the two alloys, most of the internal carbides are intragranular, intergranular carbides also appeared and developed into the interior of the two alloys. In addition, thin layers of M_7C_3 formed on Fe-19Ni-13Cr and Fe-19Ni-13Cr-2Al after exposed to 10% CH_4/H_2. Different from Fe-19Ni-13Cr, darker regions rich in Al and O appeared in the subsurface zone in Fe-19Ni-13Cr-2Al.

Similarly, the metallographic examination of the cross-sections after etching by Murakami's etchant revealed a similar morphology of the internal carburization zones for Fe-19Ni-21Cr and Fe-19Ni-21Cr-2Al after corroded in 10% CH_4/H_2 at 800°C for 12 h (Figure 4 and Figure 5). For both alloys, most of the internal carbides were intragranular and could be divided into two different layers. The outer layer had a uniform depth and contained globular carbides M_7C_3 (with M = Fe, Cr) according to the corresponding XRD results after surface grinding. The thickness of the inner layer was irregular and was larger than that of the outer layer. Carbides

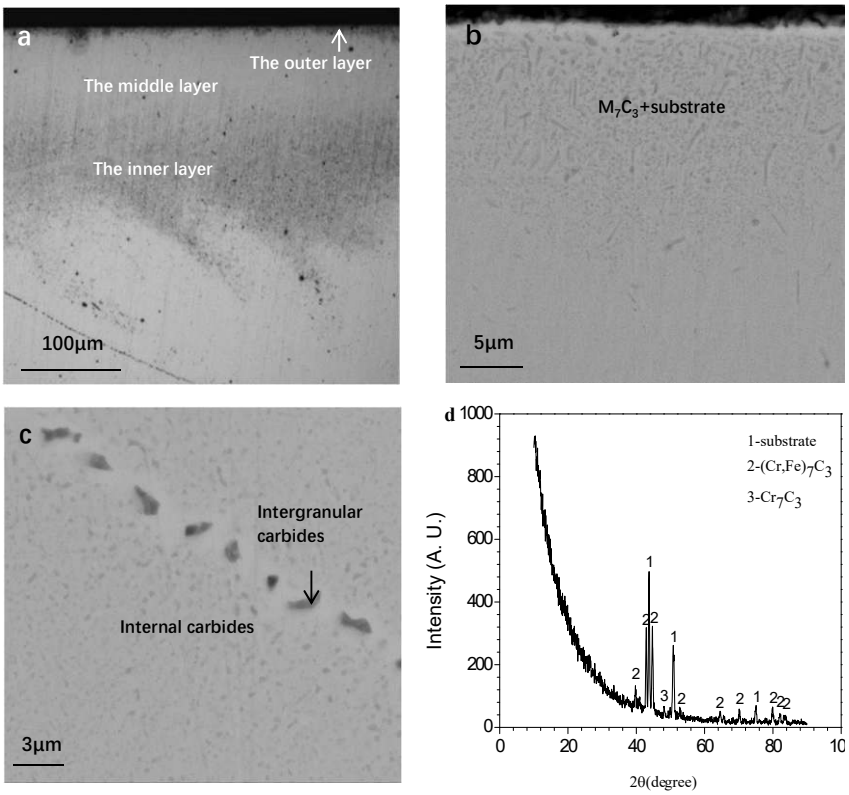

Figure 2 Micrograph of cross sections of Fe-19Ni-13Cr corroded in 10% CH_4/H_2 at 800°C for 12 h. (a) general view (OM); (b) enlarged view of the outer layer in (a) (SEM/BEI); (c) enlarged view of the inner layer in (a) (SEM/BEI); (d) XRD spectrum of the external scale.

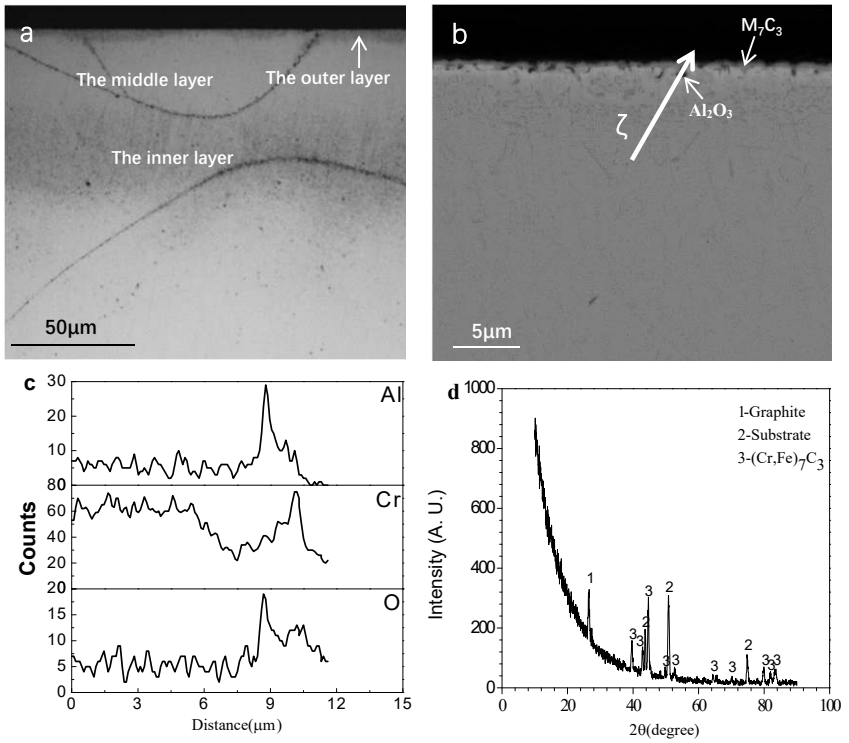

Figure 3 Micrograph of cross sections of Fe-19Ni-13Cr-2Al corroded in 10% CH_4/H_2 at 800°C for 12 h. (a) general view (OM); (b) enlarged view of the outer layer in (a) (SEM/BEI); (c) elements distribution of wave line in (b); (d) XRD spectrum of the external scale.

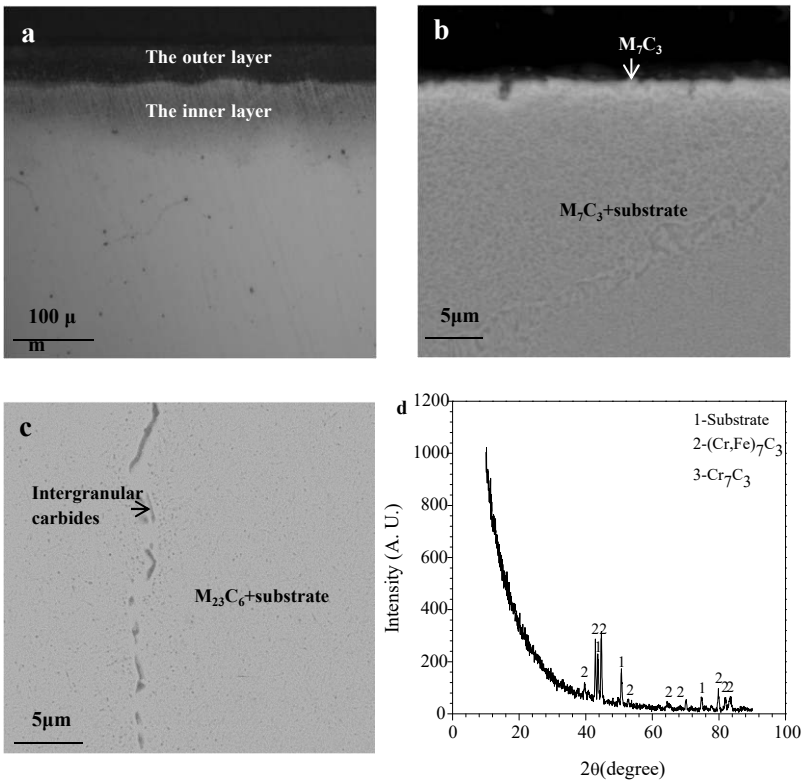

Figure 4 Micrograph of cross sections of Fe-19Ni-21Cr corroded in 10% CH_4/H_2 at 800°C for 12 h. (a) general view (OM); (b) enlarged view of the outer layer in (a) (SEM/BEI); (c) enlarged view of the inner layer in (a) (SEM/BEI); (d) XRD spectrum of the external scale.

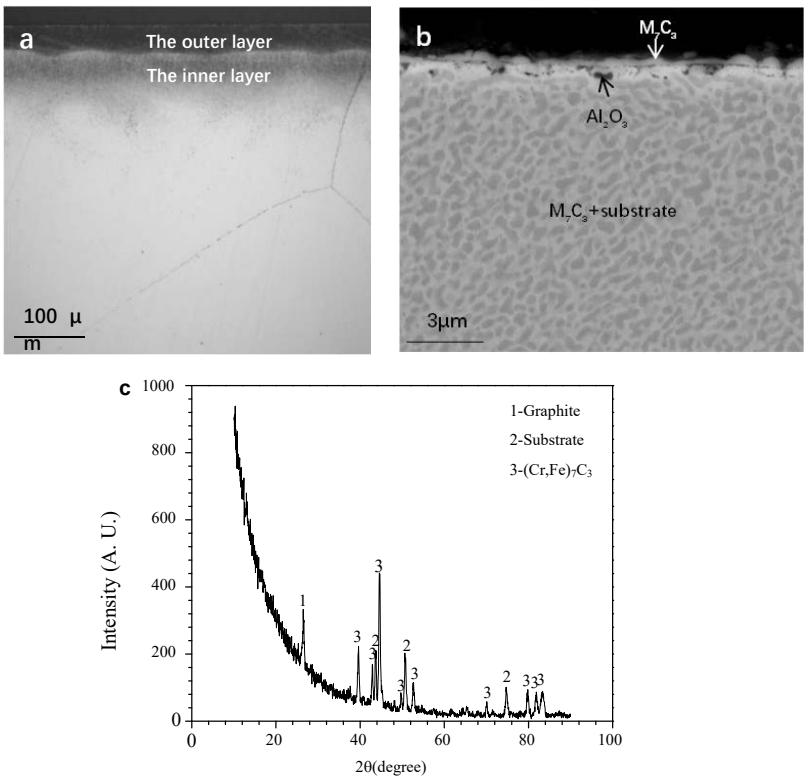

Figure 5 Micrograph of cross sections of Fe-19Ni-21Cr-2Al corroded in 10% CH_4/H_2 at 800°C for 12 h. (a) general view (OM); (b) enlarged view of the outer layer in (a) (SEM/BEI); (c) XRD spectrum of the external scale.

in the inner layer are small, cubic and need-like which could have the formula $M_{23}C_6$ (with M = Fe, Cr). Intergranular carbides also appeared and developed into the interior of the two alloys. In addition, the surface of the Fe-19Ni-21Cr was covered by a thin layer of M_7C_3. Besides the external M_7C_3 layer, internal oxide rich in Al also appeared in the subsurface zone in Fe-19Ni-21Cr-2Al.

According to Figure 6 , no internal carbides formed in Fe-19Ni-13Cr-6Al exposed to 10% CH_4/H_2 at 800°C for 12 h. For Fe-19Ni-21Cr-6Al (Figure 7), the internal carburization zone was divided into two regions. The external region had an irregular thickness and contained lots of intragranular carbides. The carbides in the inner region formed along the boundaries of the Cr-rich precipitates as described above. For the two alloys with 6 at. % Al, thin particles rich in Al and O formed on the surface of the alloys along with external carbides according to the corresponding XRD results, however, they could not be visible in the SEM micrographs due to their small sizes.

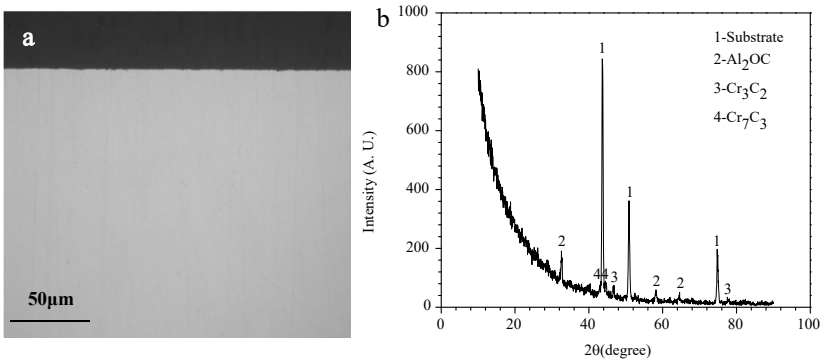

Figure 6 Micrograph of cross section of Fe-19Ni-13Cr-6Al corroded in 10% CH_4/H_2 at 800°C for 12 h. (a) general view (SEM); (b) XRD spectrum of the external scale.

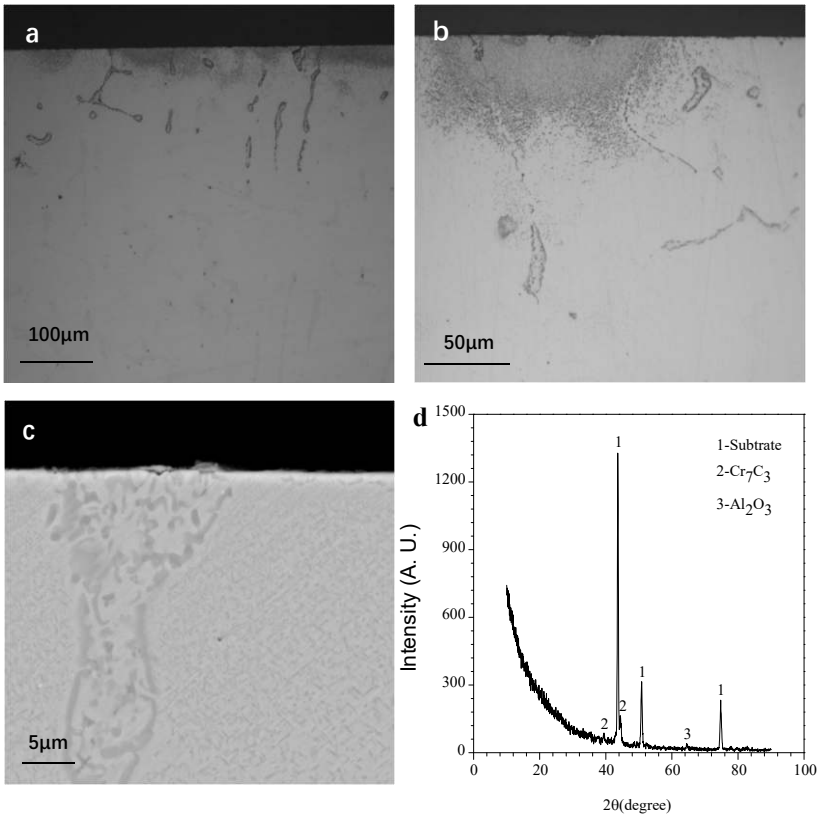

Figure 7 Micrograph of cross sections of Fe-19Ni-21Cr-6Al corroded in 10% CH_4/H_2 at 800°C for 12 h. (a) general view (OM); (b) enlarged view (OM); (c)enlarged view of the outer region(SEM/BEI); (d) XRD spectrum of the external scale.

For alloys with the same Cr content, small addition of Al (2 at. %) did not improve the corrosion resistance according to the morphology of the cross-sections. However, Fe-19Ni-21Cr-6Al suffered slighter carbon attack than other alloys. No internal carbides appeared in Fe-19Ni-13Cr-6Al, especially.

4 Discussion

The carbon activity in carburizing atmosphere composed of mixtures of CH_4 and H_2 can be calculated from the condition of equilibrium of Reaction (1). If carbon is present in its stable state (graphite), its activity is equal to unity. In this case, the equilibrium constant K_1 takes the form:

$$K_1 = \frac{P(H_2)^2_{(eq)}}{P(CH_4)_{(eq)}} \tag{3}$$

This equilibrium involving graphite is only possible if the partial pressures of H_2 and CH_4 satisfy Equation (3) with the correct value of K_1 for the temperature considered. When dealing with practical problems in which Equation (3) is generally not fulfilled, many researchers rewrite K_1 in the form:

$$K_1 = a_c \frac{P(H_2)^2}{P(CH_4)} \tag{4}$$

where $P(H_2)$ and $P(CH_4)$ are the actual partial pressures of the two gas species in the practical gas mixture, while a_c is the so-called virtual carbon activity and can be calculated by introducing the values of K_1, $P(H_2)$ and $P(CH_4)$ into Equation (4). The carbon activities calculated in this way are used to show the degree of deviation from equilibrium of Reaction (1). In particular, a_c values < 1 show that Reaction (1) should go proceed to the left so that carbon would not be deposited and, if present, should be consumed. Conversely, when $a_c > 1$ Reaction (1) should go to the right, resulting in the decomposition of CH_4 with deposition of solid carbon.

In general, the virtual carbon activity can be used to predict the actual direction of Reaction (1) and to describe the degree of deviation from equilibrium in a quantitative way. When $a_c > 1$, the higher is its value, the greater is the driving force for the carbon deposition and the more likely the probability of metal dusting.

According to the XRD results, Graphite formed on Fe-19Ni-13Cr-2Al and Fe-19Ni-21Cr-2Al. It is indicated that metal dusting occurred on these two alloys [15]. The signal of graphite was not detected by XRD analysis for Fe-19Ni-13Cr and Fe-19Ni-21Cr. However, the cross-sections of Fe-19Ni-13Cr-2Al and Fe-19Ni-13Cr show similar structure, as well as Fe-19Ni-21Cr-2Al and Fe-19Ni-21Cr. The total mass gains of the above four alloys exposed to the carburizing atmosphere used here are very close and much larger than those for alloys with 6 at. % Al. Therefore, it is more likely that metal dusting also occurs on Fe-19Ni-13Cr and Fe-19Ni-21Cr. The corresponding XRD results could not show the existence of graphite may could attribute to its small amount. The rate of carbon transfer from CH_4 at 900°C is very slow without catalyst [16]. This will lead to the appearance of linear kinetics if the carbon obtained from the decomposition of CH_4 could not be able to provide a sufficient amount of carbon atoms to diffuse into the substrate. While the corrosion kinetics of alloys without Al or with 2 at. % Al obeyed the parabolic rate after the initial stage in the presence of a Pt catalyst. The rate of decomposition of CH_4 is controlled by the decomposition of CH_3 [16]. When the flowing CH_4/H_2 gas mixture pass through the Pt catalyst, CH_4 could absorb on its surface and start to decompose. The presence of Pt catalyst may increase the rate of CH_3 decomposition effectively and therefore the rate of Reaction (1) could be improved significantly. The products (CH_3, CH_2, CH or C) might desorb from the surface of the catalyst and reach the sample surface along with the gas flow. The rates of the radical's decomposition are much faster than those of the original molecule CH_4. Therefore, Reaction (1) on the sample surface is not necessarily slow. The amount of carbon atoms produced by this reaction could sustain the diffusion of the carbon atoms into the substrate, which could result in parabolic kinetics.

The diffusion path for carbon could be established with reference to the Cr-C-O phase diagram. The related thermodynamic data could be obtained from the HSC version 6.0 [14]. However, the internal carbides formed in the Fe-Cr base alloys exposed to the gas mixture with carbon contain not only chromium but also iron. Therefore, the formula of the carbides should be M_7C_3 and $M_{23}C_6$ (M = Cr, Fe), instead of Cr_7C_83 and $Cr_{23}C_6$. The estimate of the schematic of the diffusion path of carbon could be more reliable by using the stability diagram of the quaternary M-C-O system (M = Cr, Fe). However, the thermodynamic data for M7C3 and $M_{23}C_6$ which should be used to establish the above stability diagram of M-C-O system, are very rare. Christ [17] studied the corrosion behavior of AISI 304L Fe-9Ni-18Cr carburized

for 150 h at 950°C and at $a_c = 0.9$. The average composition of the internal carbides formed in the above alloy had the formula $Fe_{7.5}Cr_{15.5}C_6$ and $Fe_{3.5}Cr_{3.5}C_3$. Christ also calculated the Gibbs free energy of formation, which could be used as an approximate estimate of the M-C-O stability diagram although the Cr/Fe ratio varies with the Fe/Ni ratio and the local carbon activity. In addition, the activity coefficients of Cr and Fe are equal to 2.3 and 1 at 950°C [17], respectively. These values could also be used here as approximate values. The calculated stability diagram for the M-C-O system is shown in Figure 8 (Fe-19Ni-12Cr-xAl) and Figure 9 (Fe-19Ni-21Cr-xAl). The dotted line a represents the dissociation pressure of Al_2O_3. For simplicity, only schematic diffusion paths, described by means of straight lines, are used here as lines b in Figure 8 and Figure 9. The diffusion paths for Fe-19Ni-13/21Cr-xAl (x = 0, 2 at. %) exposed to 10% CH_4/H_2 are seen to cross the $M_{23}C_6$ and M_7C_3 fields before entering into the graphite field. This corresponds to the experimental observation.

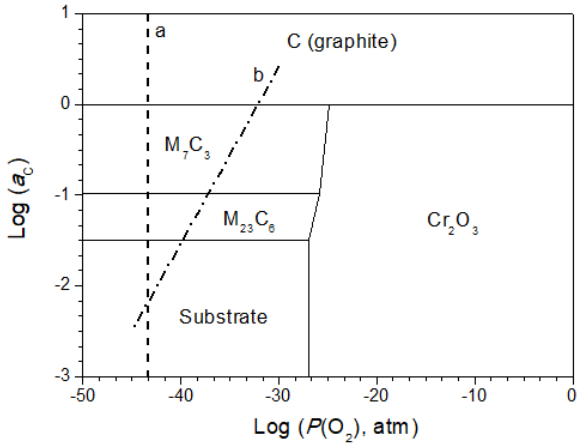

Figure 8 Calculated stability diagram for M-C-O at 800°C [16, 17]. Dotted line a: The dissociation pressure of Al_2O_3; Dot-dashed line b: Schematic view of the diffusion path for Fe-19Ni-13Cr-xAl (x = 0, 2 at. %) exposed to 10% CH_4/H_2

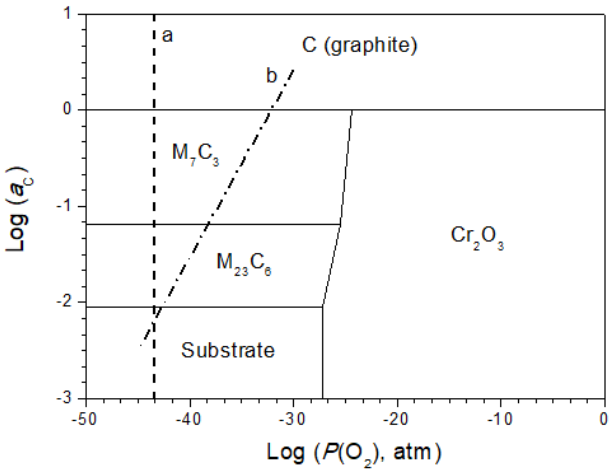

Figure 9 Calculated stability diagram for M-C-O at 800°C [16, 17]. Dotted line a: The dissociation pressure of Al_2O_3; Dot-dashed line b: Schematic view of the diffusion path for Fe-19Ni-21Cr-xAl (x = 0, 2 at. %) exposed to 10% CH_4/H_2

The morphology of the internal carburization zones for Fe-19Ni-21Cr and Fe-19Ni-21Cr-2Al is common. Many papers have reported and investigated this traditional two-layer internal carburization zone formed in heat-resisting alloys with M_7C_3 in the outer layer and $M_{23}C_6$ in the inner layer [18, 19]. However, few articles have described the three-layer internal carburization zones formed in Fe-19Ni-13Cr and Fe-19Ni-13Cr-2Al. Essentially there are only two layers formed in Fe-19Ni-13Cr and Fe-19Ni-13Cr-2Al with M_7C_3 in the outer layer and $M_{23}C_6$ in the inner layer, just like Fe-19Ni-21Cr and Fe-19Ni-21Cr-2Al. However, due to the small size of $M_{23}C_6$ near the outer layer, OM could not detect their presence, virtual three-layer internal carburization zones appeared. The quantity and the volume of the carbides vary with the distance away from the alloy/scale interface [20]. Carbides in the outer layer, which have the largest

volume, are proved to be M_7C_3 by the XRD analysis after surface griding. Then the volume of the carbides reduced, and the amount increased dramatically in the middle layer. Carbides in this layer were too small to be detected by the optical microscope. Although the carbides in the inner layer also have the formula $M_{23}C_6$, they grow bigger than those in the middle layer, but the number of the carbides decreases. According to Neil [20], the size of the internal carbides could be affected by many factors. The nucleation rate of the carbides increases with the improvement of the absolute value of standard free energy for carbides formation. Therefore, the size of M_7C_3 particles in the outer layer is larger than that of $M_{23}C_6$ in the other two layers.

The kinetic curves for all alloys exposed to the carburizing atmosphere used here obey the parabolic rate law. For Al-free alloys and alloys with 2 at. % Al, large number of internal carbides formed, and the internal carburization of these alloys was controlled by lattice diffusion of carbon through the depleted metal matrix. No internal carbides formed in Fe-19Ni-13Cr-6Al and external particles rich in Al and O appeared. Therefore, diffusion of aluminum may control the whole process. For Fe-19Ni-21Cr-6Al, thin external Al_2O_3 and the internal carbides formed simultaneously. It is unclear that which diffusion process should be responsible for the parabolic rate law.

The effect of Al could be evaluated by comparing the corrosion behavior of alloys presenting similar iron, nickel and chromium contents, but different aluminum contents exposed to the carburizing atmosphere. Small addition of Al (2 at. %) resulting in slightly decrease of the mass gain did not improve the corrosion resistance significantly, and the morphology of the corresponding cross-sections for Al-free alloy and the alloy with 2 at. % Al with the same chromium content are similar. Large addition of Al (6 at. %) affect the corrosion behaviors significantly. The resistance to carbon attack was enhanced. Although the nominal content of the gas mixture used here did not contain oxidant O, impurities still existed which could produce oxygen pressure sufficient to form alumina. The solubility of carbon in Al_2O_3 is below 0.01 ppm [21]. Therefore, a continuous Al_2O_3 scale formed on alloy could provide an effective barrier to the carbon attack. 2 at. % Al was too low to form a continuous, protective Al_2O_3 scale and only led to the formation of internal alumina which could not hinder the carbon attack effectively. No internal carbide formed in Fe-19Ni-13Cr-6Al and the XRD result showed the existence of products rich in Al and O. Therefore, a protective scale formed on this alloy which could protect the substrate from the carbon attack totally. 6 at. % addition of Al to the alloy presenting 21 at. % Cr still improve the corrosion resistance significantly due to the existence of the external alumina, but not totally. Internal carbides still existed in Fe-19Ni-21Cr-6Al. Therefore, 6 at. % Al was not enough for alloys presenting 21 at. % Cr exposed to this carburizing atmosphere. In the initial stage, alumina and carbides formed on the metal surface. External carbides were not protective and was permeable to the gas. Carbon atoms could diffuse inwards through the external carbides or the bare surface. However, the amount and the volume of the external carbides formed on Fe-19Ni-13Cr-6Al was less than those on Fe-19Ni-21Cr-6Al. Therefore, although containing same Al content, protective scale formed on Fe-19Ni-13Cr-6Al, internal carbides still existed in Fe-19Ni-21Cr-6Al.

5 Conclusions

The corrosion behaviors of Fe-19Ni-13/21Cr-xAl (x = 0, 2, 6 at. %) alloys in a 10% CH_4/H_2 gas mixture at 800°C were studied. 2 at. % Al addition did not affect the corrosion resistance obviously. A further addition up to 6 at. % Al produced a significant decrease of the rate of attack, even the internal carburization disappeared in Fe-19Ni-13Cr-6Al. However, 6 at. % Al was still insufficient to maintain the formation of protective alumina scales for alloys with 21 at. % Cr. Therefore, more Al should be needed for this class of ternary alloys to obtain a complete prevention of the carbon attack.

An addition of Cr from 13 at. % up to 21 at. % affect the appearance of the internal carburization zone under the optical microscope. Less Cr content is helpful for alloys with 6 at. % Al exposed to the carburizing atmosphere with oxygen pressure insufficient to form chromia to obtain better corrosion resistance.

Acknowledgements

This work was financially supported by NSFC (Grant No. 51801026), the Foundation for Young Talents of Shenzhen Polytechnic (Grant No. 601822K35018), Foundation for Young Talents in Higher Education of Guangdong (Grant No. 601821K35055).

References

[1] Rahmel A, Grabke HJ and Steinkusch W. Carburization-introductory survey. Materials and Corrosion, 1998, **49**(4): 221-225. https://ur.booksc.org/book/127940/b9421d

[2] Grabke HJ. Thermodynamics, mechanisms and kinetics of metal dusting. Materials and Corrosion, 1998, **49**(5): 303-308. https://doi.org/10.1002/(SICI)1521-4176(199805)49:5⟨303::AID-MACO303⟩3.0.CO;2-P

[3] Gheno T, Monceau D, Zhang JQ, *et al*. Carburisation of ferritic Fe-Cr alloys by low carbon activity gases. Corrosion Science, 2011, **53**(9): 2767-2777. https://doi.org/10.1016/j.corsci.2011.05.013

[4] Salas O, Melo-Maximo DV, Oseguera J, *et al*. Role of PVD oxide coatings on HK40 cast steel during short and long exposure to C-rich atmospheres. Materials Characterization, 2013, **83**: 58-67. https://doi.org/10.1016/j.matchar.2013.05.016

[5] Olivares RI, Young DJ, Nguyen TD, *et al*. Resistance of High-Nickel, Heat-Resisting Alloys to Air and to Supercritical CO_2 at High Temperatures. Oxidation of Metals, 2018, **90**: 1-25. https://doi.org/10.1007/s11085-017-9820-7

[6] Nguyena TD, Fontaine AL, Yang LM, *et al*. Atom probe study of impurity segregation at grain boundaries in chromia scales grown in CO_2 gas. Corrosion Science, 2018, **132**: 125-135. https://doi.org/10.1016/j.corsci.2017.12.024

[7] Young DJ and Zhang JQ. Alloy Corrosion by Hot CO_2 Gases. JOM, 2018, **70**: 1493-1501. https://doi.org/10.1007/s11837-018-2944-7

[8] Yamamoto Y, Brady MP, Lu ZP, *et al*. Creep-resistant, Al_2O_3-forming austenitic stainless steels, Science, 2007, **316**(5823): 433-436. https://doi.org/10.1126/science.1137711

[9] Mitchell DRG and Young DJ. The effect of molybdenum and aluminum additions on the carburization behavior of high temperature steel. Journal of Materials Science Letters, 1993, **12**: 1076-1079. https://doi.org/10.1007/BF00420526

[10] Becker P and Young DJ. Carburization resistance of nickel-base, heat-resisting alloys. Oxidation of Metals, 2007, **67**: 267-277. https://doi.org/10.1007/s11085-007-9058-x

[11] Allam IM. Carburization/oxidation behavior of alloy Haynes-214 in methane-hydrogen gas mixtures. Oxidation of Metals, 2009, **72**: 127-144. https://doi.org/10.1007/s11085-009-9151-4

[12] Liu S, Guo QQ, Wu XF, *et al*. Carburization of three Fe-19Ni-21Cr-xAl (x = 0, 2, 6 at.%) alloys at 900°C in oxygen-contaminated CH_4/H_2 atmospheres, Corrosion Science, 2016, **111**: 436-445. https://doi.org/10.1016/j.corsci.2016.05.008

[13] Liu S, Shen J, Wu XF, *et al*. The effect of sulphur on the carburization of three Fe-19Ni-13Cr alloys with various Al additions at 900°C in oxygen-contaminated CH_4-H_2-H_2S atmospheres, Corrosion Science, 2016, **112**: 94-109. https://doi.org/10.1016/j.corsci.2016.07.012

[14] Roine A. HSA Chemistry Version 6.0, Outokumpu Research, Oy, Finland, 2006.

[15] Young DJ. High Temperature Oxidation and Corrosion of Metal, 1st ed., Elsevier, Great Britain, 2008.

[16] Grabke HJ. Carburization carbide formation, metal dusting, coking. Materials Technology, 2002, **36**: 297-305.

[17] Christ HJ. Experimental characterization and computer-based description of the carburization behaviour of the austenitic stainless steel AISI 304L, Materials and Corrosion, 1998, **49**(4): 258-265. https://doi.org/10.1002/(SICI)1521-4176(199804)49:4⟨258::AID-MACO258⟩3.0.CO;2-U

[18] Udyavar M and Young DJ. Precipitate morphologies and growth kinetics in the internal carburisation and nitridation of Fe-Ni-Cr alloys. Corrosion Science, 2000, **42**(5): 861-883. https://doi.org/10.1016/S0010-938X(99)00095-5

[19] Smith GM, Young DJ and Trimm DL. Carburization kinetics of heat-resistant steels. Oxidation of Metals, 1982, **18**: 229-243. https://doi.org/10.1007/BF00656570

[20] Birks N, Meier GH and Pettit FS. Introduction to the High-Temperature Oxidation of Metals, 2nd ed., Cambridge University Press, United Kingdom, 2006.

[21] Young DJ and Zhang J. Metal dusting: catastrophic corrosion by carbon. JOM, 2012, **64**: 1461-1469. https://doi.org/10.1007/s11837-012-0476-0